Characterization and Modeling of Polyoxometalate-based Ionic Liquids. Force Field Refinement and Insights into their Dynamical Behavior

Khaoula Merimi,[a] Albert Masip-Sánchez,[a] Nour Zeaiter,[b,c] Franck Camerel,[d] Betty Cottyn-Boitte,[c] Catherine Roch-Marchal,[b] Sébastien Floquet,[b] Xavier López[a]*

[a] *Departament de Química Física i Inorgànica, Universitat Rovira i Virgili, Marcel·lí Domingo 1, 43007 Tarragona, Spain*

[b] *Institut Lavoisier de Versailles, UMR 8180, Université de Versailles St-Quentin en Yvelines, CNRS, Université Paris-Saclay, 78035 Versailles, France*

[c] *Université Paris-Saclay, INRAE, AgroParisTech, Institute Jean-Pierre Bourgin for Plant Sciences (IJPB), 78000, Versailles, France*

[d] *Univ Rennes, CNRS, ISCR (Institut des Sciences Chimiques de Rennes) - UMR 6226, 35000 Rennes, France*

E-mail: javier.lopez@urv.cat

ABSTRACT

Ionic liquids (ILs) are salts with melting points below 100°C, being a more sustainable alternative to organic solvents because of their negligible vapor pressure and high thermal stability. The recently developed branch of polyoxometalate-based ILs (POM-ILs) incorporates the unique properties (redox, catalytic) of POMs to the advantages of ILs, opening the door to further advancements and applications in the field. In the present work we have synthesized and characterized new POM-ILs. Motivated by this progress and building upon current knowledge on simulations of classical ILs, we also propose a computational setup to describe the dynamic behavior of bulk POM-ILs through atomistic molecular dynamics simulations. The cationic part is an organic PR_4^+ unit, and POMs are well-known systems such as Lindqvist, Keggin and Wells-Dawson, among others. Part of the work presents variations made to the (reference) AMBER force field atomic parameters σ and ε, and their justification. We observe that changes applied remarkably affect the molecular mobilities (diffusivities or viscosities) of the system. Our analysis establishes that one set of the tested parameters reproduces the relative experimental viscosities for the family of compounds analyzed. Taking this setup, we further describe computationally the local and bulk dynamical properties, detailing the anion-cation interactions. One remarkable fact is that the experimental diffusivities are reproduced with very little microscopic molecular motion, that is, the mobility of the constituent parts is very limited, mostly restricted to a local position.

INTRODUCTION

Ionic liquids (ILs) are complex molecular salts typically composed of bulky, asymmetric and flexible organic cations combined with either organic or inorganic anions. They exhibit low lattice energy and high conformational entropy, which confers them a unique property: a melting point below 100°C, allowing them to remain liquid near room temperature.[1-4] The appealing properties of ILs include high thermal stability, excellent ionic conductivity, and negligible vapor pressure, making them ideal alternatives to conventional volatile organic solvents. Also referred to as "designer solvents", ILs have garnered attention for their tunable solvation and coordination properties, tailored by the choice of ions.[5-6] They exhibit a complex behavior that depends on the predominant interactions (significant short-range van der Waals interactions and strong long-range Coulombic forces) as well as their heterogeneous dynamics with extended relaxation times. Consequently, both theoretical and experimental studies of ILs are greatly challenging.[3,7-8]

ILs have been extensively studied by means of simulations at various computational levels, ranging from *ab initio* molecular dynamics (AIMD) and molecular simulations with polarizable force fields to the classical molecular dynamics (MD) and Monte Carlo simulations.[9-10] These simulations are often complemented by statical thermodynamics and quantum mechanical calculations, such as density functional theory (DFT), providing insight into intra- and intermolecular interactions.[11] Recent research based on molecular simulations of ILs highlights the growing use of multiscale approaches, including classical MD combined with DFT, or standalone AIMD, to address the structural complexity of ILs. Such methods require advanced strategies to overcome the significant computational demand.[12]

Polyoxometalate-based ionic liquids (POM-ILs), despite very limited research to date,[13-16] have positive prospects due to their unique structural diversity and intrinsic physicochemical properties of polyoxometalates (POMs, the anionic part). POMs are nano-sized polymetallic oxides predominantly composed of early transition metals in high oxidation states. These compounds are typically polyanionic and adopt frameworks built upon pseudo-octahedral MO_6 units. These arrangements, combined with variable charge density, solubility in a range of solvents, redox flexibility, and chemical stability, give POMs a wide range of functionalities, forming the basis for their many applications. These are especially well known in electrochemistry,[17] catalysis,[15,18] materials science,[19] supramolecular chemistry,[20] and nanotechnology.[21] These compounds have also been used in the development of reactive wares and thermotropic liquid crystals.[16,22-24] Furthermore, POMs offer significant advantages owing to their remarkable versatility. Their physical and chemical properties, including anionic charge, can be tailored by modifying the molecular architecture and composition, grafting organic or organometallic moieties, or coordination with transition metals and inorganic complexes. Thanks to the inherent tunability of ILs, enabled by numerous combinations of cations their functionalization, POM-ILs emerge as multifunctional soft materials that integrate the properties of both ILs and POMs.

POM-ILs could therefore significantly contribute to modern chemistry and challenges of today.[12,14,16,25] Among the various potential applications of POM-ILs, Zeaiter et al.,[26] recently illustrated their dual role s solvent and catalyst in the valorization of recalcitrant residues from biorefineries. In a different context, Mitchell and coworkers[27-28] demonstrated the use of POM-ILs anticorrosive coatings for the protection and preservation of cultural heritage materials.

At variance with the extensive theoretical studies on conventional ILs, POM-ILs remain unexplored at the computational level. Previous computational studies on ILs have primarily relied on classical atomistic force fields[1,3,9,29] although more sophisticated approaches are available (albeit at significantly higher computational cost). The structural and electronic complexity of POMs, along with their large molecular size, have significantly impact on the computational effort required for accurate simulations.[30] Despite these challenges, MD simulations remain a powerful tool for investigating and predicting properties of POM-ILs, provided they are applied appropriately. However, their accuracy heavily relies on the simulation settings, particularly the force field parameters governing non-bonded interatomic interactions, which lay a dominant role in the behavior of such systems.[1,31-33] Furthermore, the unique characteristics of POMs, such as their high negative charge and distinct stoichiometries, further amplify these effects, diverging significantly from the ±1 monovalent ion pairs found in conventional ILs.[11]

Over the past few decades, force fields have been developed and parameterized for ILs using existing models such as OPLS,[34] CHARMM,[35] AMBER or GAFF.[9,36] Notably, Canongia Lopes and co-workers have optimized several force fields, including the Canongia Lopes and Padua (CL&P) force field,[37] based on the OPLS-AA and AMBER frameworks, to accurately reproduce experimental data for a wide variety of ILs composed of relatively small organic molecules. However, these established force fields do not account for POM-ILs. In this study, we have employed an AMBER-based force field previously optimized by our group for MD involving POMs, which has been widely used[38-40] and has proven robust in describing the structural and dynamic properties of POMs in solution.[41]

Herein, we present a MD-based computational study on POM-ILs, motivated by recent experimental work which identifies specific cation-POM combinations exhibiting diverse ionic liquid behavior. The physicochemical properties were characterized and their applicability as catalysts explored.[14-15,26] However, catalytic applications in mild chemical conditions require POM-ILs that are fluid at low temperatures (20–90°C) and, to date, in lack of any predictive model, it is necessary to synthesize a large number of POM-ILs to determine the most appropriate ones. This is a time-consuming experimental task and, thus, simulation tools would undoubtedly save time and make it possible to better target POM-ILs that are potentially interesting for various applications. We explore and propose the computational settings to theoretically reproduce and compare the bulk dynamic

behavior of several POM-ILs, complementing the experimental studies and establishing a benchmark for future computational works on POM-ILs.

METHODOLOGY AND COMPUTATIONAL DETAILS

Syntheses and characterization of POM-based ionic liquids

The syntheses and characterizations of POMs and POM-ILs were performed as described by Martinetto et al.[14-15] Additional details on these procedures are given in the electronic supporting information (ESI).

Fourier Transform Infrared (FT-IR) spectra. These were recorded on a 6700 FT-IR Nicolet spectrophotometer, using diamond ATR technique. The spectra were recorded on non-diluted compounds and ATR correction was applied.

ThermoGravimetric Analysis (TGA). Measurements were recorded on a Seiko TG/DTA 320 thermogravimetric balance. The samples were measured between room temperature and 700°C (scan rate: 5°C min^{-1}, under O_2).

Nuclear magnetic resonance (NMR). ^{1}H (300 MHz) NMR and ^{31}P (121,5 MHz) NMR spectra were recorded at room temperature on a Bruker AC-300 spectrometer in $(CD_3)_2CO$, CD_3OD and $(CD_3)_2SO$. Chemical shifts are reported in parts per million (ppm) relative to internal references. The residual peaks is at 2.05 ppm of $(CD_3)_2CO$, 3.31 ppm for CD_3OD and 2.5 ppm for $(CD_3)_2SO$ on the ^{1}H (300 MHz) NMR spectra. Liquid ^{183}W NMR spectra were obtained on a high resolution 400 MHz Bruker Avance spectrometer, equipped with 10 mm BBO probes. CD_3CN was used as a solvent. Spectra were measured in 10 mm tubes at a Larmor frequency of 16.7 MHz for the ^{183}W.

Differential scanning calorimetry (DSC). Measurements were performed on a NETZSCH DSC 200 F3 instrument equipped with an N_2 cooler, allowing measurements from –170°C up to 450°C. The samples were examined at a scanning rate of 10°C min^{-1} by applying two heating and one cooling cycles. The apparatus was calibrated with indium (156.6°C).

Phase behavior was studied by *Polarized light Optical Microscopy* on a Nikon H600L polarizing microscope equipped with a Linkam “liquid crystal pro system” hotstage LTS420.

Viscosity measurements were performed on a Thermofischer Haake MARS III controlled-stress rheometer equipped with a cone-plate geometry (diameter = 35 mm, angle = 1°) and a Peltier thermal regulator.

Computational details

Quantum Mechanical calculations. The geometries of the constituent molecules of the systems herein discussed were fully optimized at the DFT level with the Gaussian16 revision A.03 software package[42] using the B3LYP hybrid functional[43] for POMs and the BP86 functional for cations.[44] The electrons were

described using double-ζ+polarization basis sets: 6-31G(d,p) for H, C, O and P, and LANL2DZ+polarization for Mo and W.[45-46] In addition, dispersion corrections were included using Grimme's D3BJ method.[47] For the optimization step, the molecular environment was approximated by the Polarizable Continuum Model (PCM).[48] The atomic charges necessary for MD simulations, i.e. ChelpG (Charges from Electrostatic Potentials), were derived from single point solvent-free DFT calculations using the Gaussian16 package with the B3LYP. For additional analysis, Bader charges were computed using the Multiwfn 3.4.1 software.[49]

Classical Molecular Dynamics simulations. We performed atomistic MD simulations using the GROMACS 2019.3 package[50] with a cubic simulation box and periodic boundary conditions. Electrostatic and van der Waals interactions were truncated at real-space cutoff of 1.4 nm to minimize artifacts. Long-range electrostatic interactions were handled with the Smooth Particle-Mesh Ewald (SPME) method,[51] with a Fourier grid spacing of 0.12 nm to ensure an accurate treatment of electrostatics. All the simulation boxes contain 100 randomly placed POM units along with the corresponding cations to ensure electroneutrality. Simulations were conducted at T = 350 K, unless otherwise specified, which lies within the (semi)liquid range of the studied systems. The temperature coupling was handled separately for the POM anions and cations using different thermostats, with coupling times set to 0.02 ps for the POMs and 0.1 ps for the cations.

Firstly, an energy minimization of the mentioned box was performed, followed by a multi-step equilibration protocol. The initial equilibration phase involved a series of 1 ns simulations in isothermal-isobaric (*NPT*) and the canonical (*NVT*) ensembles. The process began with an *NPT* simulation at 10 bar to compact all the system components, maintaining the target temperature using a Nosé-Hoover[52, 53] thermostat and a Parrinello-Rahman barostat[54] with a pressure coupling time of 5 ps. This was followed by an intermediate *NPT* simulation at 5 bar to further adjust the pressure under the same conditions. Finally, an *NPT* simulation at atmospheric pressure (1 bar) was performed using a Berendsen thermostat and barostat to achieve the correct density and prevent the formation of unrealistic void bubbles. Before proceeding to the production stage of the simulation, a 1 ns *NVT* simulation was carried out to further stabilize the system at the target temperature, using Berendsen thermostat.[55] The production run is characterized by a 40 ns *NVT* simulation (and a time step of 1 fs for numerical integration) with temperature controlled by the velocity rescaling algorithm with stochastic term (v-rescale).[56] From this, the last 20 ns were used for analysis to ensure a fully equilibrated system. To account for statical variability, the entire procedure was duplicated from different initial configurations.

Atomistic Force Field Parameters. For the molecular dynamics simulations, POM-IL systems are represented by the classical AMBER18 force field for cations and a modified AMBER for POMs, as adapted from a previous work.[41] In this model, non-bonding interactions are handled by treating the

atoms with the 12-6 Lennard-Jones (LJ) potential. The short-range interactions between atoms *i* and *j*, including van der Waals forces, Pauli repulsion and dispersion, are captured by a single pairwise additive potential represented by equation 1:

$$E_{LJ}^{ij} = 4\varepsilon_{ij}\left[\left(\frac{\sigma_{ij}}{r_{ij}}\right)^{12} - \left(\frac{\sigma_{ij}}{r_{ij}}\right)^{6}\right] \quad (1)$$

where the cross-interaction *ij* parameters are obtained by applying the Lorentz-Berthelot combination rules (equations 2 and 3):

$$\sigma_{ij} = \left(\frac{\sigma_i + \sigma_j}{2}\right) \quad (2)$$

$$\varepsilon_{ij} = \sqrt{\varepsilon_i \varepsilon_j} \quad (3)$$

These rules combine the sigma (σ) and epsilon (ε) parameters of each atom specified in the force field. An accurate choice of σ and ε is essential, as they define fundamentally the shape of the LJ potential and, hence, the behavior of the system. σ is a geometrical parameter related to the atom size, linked to the interatomic distance (*r*) such that the potential minimum is given by $r_{min} = 2^{1/6}\,\sigma$. The ε parameter describes the depth of the LJ potential well.

RESULTS AND DISCUSSION

A. Synthesis and physical properties of POM-ILs

POM-ILs can associate a huge variety of cations and POMs. In this study, for the cationic part, we focus only on POM-ILs containing tributyl(hexadecyl)phosphonium ($P_{4,4,4,16}^{+}$) and trihexyl(tetradecyl)phosphonium ($P_{6,6,6,14}^{+}$) cations. Particularly, the tributyl(decyl)phosphonium ($P_{4,4,4,10}^{+}$) cation was employed exclusively in combination with the [$W_6O_{19}^{2-}$] anion. The POM-ILs were either synthesized in this work or reported by Rickert et al.[57] and Martinetto et al.[14-15] For these salts, the resulting POM-ILs usually appear indeed much more fluidic than imidazolium or tetraalkylammonium analogues.[58] For the anionic part, we selected POMs for which the charges vary from –3 to –12 and mainly tungstic POMs which are usually more stable with temperature in POM-ILs:[14] four isopolyoxotungstates [$W_6O_{19}^{2-}$], [$W_{10}O_{32}^{4-}$], [$H_2W_{12}O_{40}^{6-}$] and [$H_2W_{12}O_{42}^{10-}$] and four phosphotungstic/molybdic POMs [$PW_{12}O_{40}^{3-}$], [$PW_{11}O_{39}^{7-}$], [$P_2W_{18}O_{62}^{6-}$] and [$P_2Mo_{18}O_{62}^{6-}$]. All the components studied are shown in Figure 1.

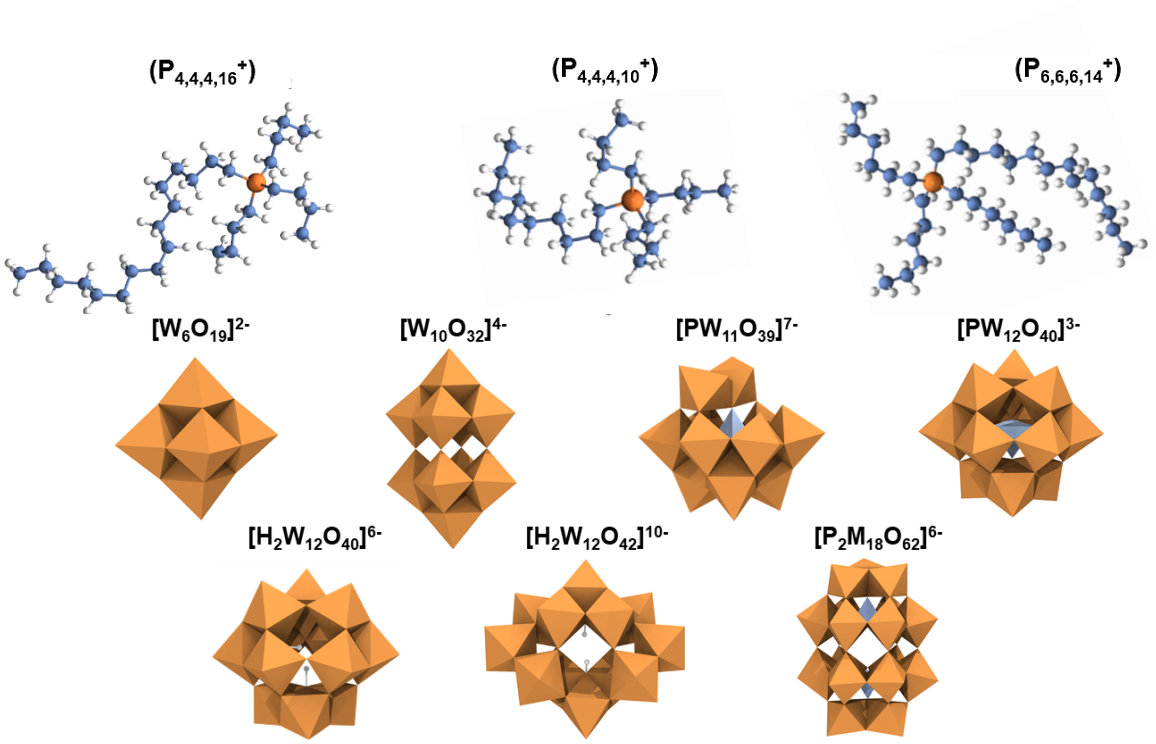

Figure 1. Ions composing the POM-ILs analyzed. The nomenclature of cations follows the number of carbon atoms of the PR_4^+ alkyl chains (ball-and-stick view: phosphorus – orange, carbon – blue and hydrogen – white). For polyoxometalates, each octahedron corresponds to MO_6 (M = W or Mo).

As previously described by Martinetto et al., the POM-ILs are prepared either by ion exchange method or by direct synthesis.[14-15] The POM-ILs are isolated as a viscous liquid or a solid phase, separated, washed by water and then dried under vacuum. The crude products can still contain an excess of the starting phosphonium salt which is eliminated by passing the POM-ILs on a steric exclusion column (SEC) using THF as solvent. The final materials were characterized by FT-IR, NMR (^{183}W, ^{1}H, ^{31}P nuclei), and TGA to confirm preservation of the POM moiety, demonstrate successful formation of the POM-IL assemblies, and determine the number of counter-cations per POM unit (see the ESI for additional data). In this work the combinations $(P_{4,4,4,16})_3[PW_{12}O_{40}]$, $(P_{4,4,4,16})_7[PW_{11}O_{39}]$, $(P_{6,6,6,14})_7[PW_{11}O_{39}]$, $(P_{4,4,4,16})_6[P_2W_{18}O_{62}]$, $(P_{6,6,6,14})_6[P_2W_{18}O_{62}]$, $(P_{6,6,6,14})_6[H_2W_{12}O_{40}]$, $(P_{6,6,6,14})_{10}[H_2W_{12}O_{42}]$ were prepared and characterized. The other POM-ILs are extracted from the literature.

For these POM-ILs, the glass transition and melting point temperatures (Table 1) were determined by DSC measurements under N_2, while polarized optical microscopy pictures taken above and below T_g were used to confirm the nature of the transition and the isotropic nature of the liquid after melting point. Qualitatively, the charge of the POMs clearly influences the melting points of the compounds. The most charged POM-ILs seems to display lower T_g values; however, we could not establish a clear empirical correlation between T_g and the charge density of the POMs. This strongly suggests that

additional parameters are involved, justifying the development of a theoretical model to predict the behaviour of these POM-ILs.

Table 1. Experimental Glass transition temperatures (DSC), aspect at room temperature and viscosity measurements at 298 and 373 K for various phosphonium based POM-ILs relevant for the present work.

System	T_g/T_f (K)	Viscosity (Pa·s)		Aspect at room temperature	Reference
		298 K	373 K		
$(P_{4,4,4,16}^+)_2[W_6O_{19}^{2-}]$	328*	-	-	-	57
$(P_{6,6,6,14}^+)_2[W_6O_{19}^{2-}]$	225	2	-	Viscous liquid	59
$(P_{6,6,6,14}^+)_3[PW_{12}O_{40}^{3-}]$	313/373*	-	-	Highly Viscous gel (ionic liquid crystal)	This work
$(P_{4,4,4,16}^+)_3[PW_{12}O_{40}^{3-}]$	372*	>20000	-	Solid	57
$(P_{6,6,6,14}^+)_6[H_2W_{12}O_{40}^{6-}]$	253	325	0.9	Slightly Viscous liquid	This work
$(P_{6,6,6,14}^+)_{10}[H_2W_{12}O_{42}^{10-}]$	200	3.84	0.09	Liquid	This work
$(P_{6,6,6,14}^+)_7[PW_{11}O_{39}^{7-}]$	196	27.5	0.25	Viscous Material	This work
$(P_{4,4,4,16}^+)_7[PW_{11}O_{39}^{7-}]$	230	760	1.6	Viscous liquid	This work
$(P_{6,6,6,14}^+)_4[W_{10}O_{32}^{4-}]$	263	2200	0.3	Viscous liquid	15
$(P_{6,6,6,14}^+)_6[P_2Mo_{18}O_{62}^{6-}]$	272	19500	19	Viscous gel	14
$(P_{4,4,4,16}^+)_6[P_2Mo_{18}O_{62}^{6-}]$	213	17460[a]	50	Highly viscous gel	This work
$(P_{6,6,6,14}^+)_6[P_2W_{18}O_{62}^{6-}]$	416	3300	217	Viscous gel (ionic liquid crystal)	This work
$(P_{6,6,6,14}^+)[Cl^-]$	223*	0.86	0.04	Liquid	60
$(oMIM^+)[tF_2N^-]$	-	0.091	-	Liquid	9

[a] Determined at 313 K.

Viscosity (η) measurements for the POM-ILs were carried out between 20 and 100°C (293 and 373 K). The experimental temperature dependence of viscosity is shown in Figure 2, while selected values at 298 and 373 K are summarized in Table 1. This property dramatically varies between POM-ILs. Interestingly, the most fluidic combination corresponds to the most charged POMs, namely $(P_{6,6,6,14}^+)_6[H_2W_{12}O_{40}^{6-}]$ and $(P_{6,6,6,14}^+)_{10}[H_2W_{12}O_{42}^{10-}]$. For instance, the viscosity of $(P_{6,6,6,14}^+)_{10}[H_2W_{12}O_{42}^{10-}]$ at room temperature is around 3.84 Pa·s, similar to that of typical shampoo (3.00 Pa·s) and comparable with the viscosity of $(P_{6,6,6,14})[Cl^-]$ at room temperature (0.9 Pa·s). As a general feature,

upon temperature increases, the viscosity gradually decreases and falls to 0.09 Pa·s at 373K for $(P_{6,6,6,14}^{+})_{10}[H_2W_{12}O_{42}]^{10-}$, a value close to the viscosity of orange juice.

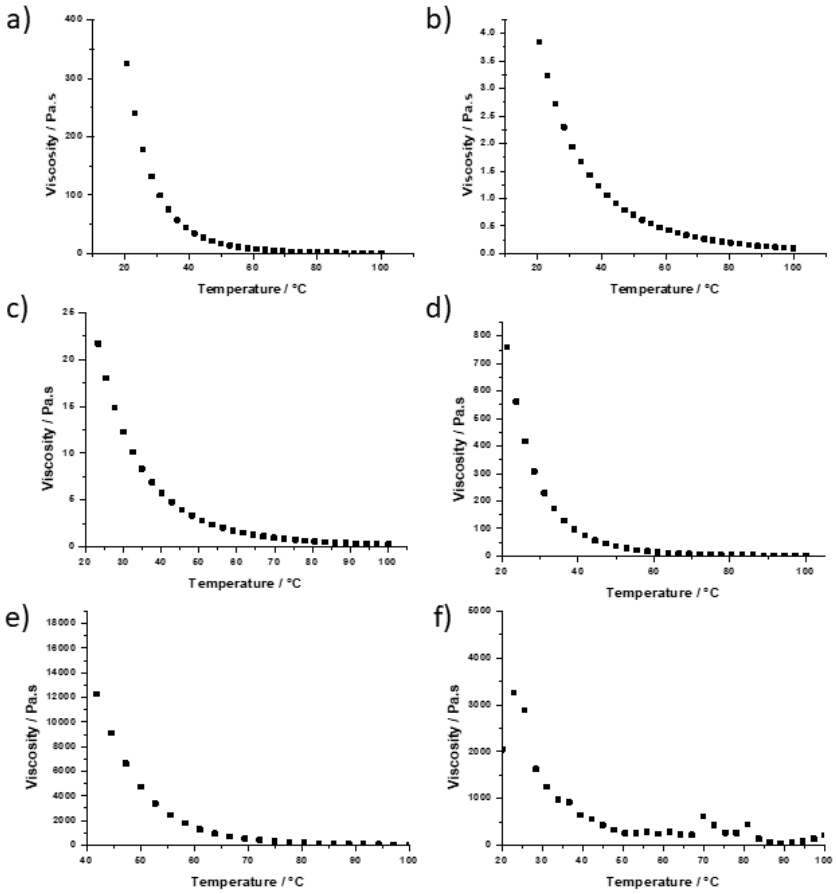

Figure 1. Viscosity of newly reported compounds as a function of temperature between 20°C and 100°C (293 K to 373 K) (γ = 10 s^{-1}): a) $(P_{6,6,6,14}^{+})_6[H_2W_{12}O_{40}^{6-}]$; b) $(P_{6,6,6,14}^{+})_{10}[H_2W_{12}O_{42}^{10-}]$; c) $(P_{6,6,6,14}^{+})_7[PW_{11}O_{39}^{7-}]$; d) $(P_{4,4,4,16}^{+})_7[PW_{11}O_{39}^{7-}]$; e) $(P_{4,4,4,16}^{+})_6[P_2Mo_{18}O_{62}^{6-}]$; f) $(P_{6,6,6,14}^{+})_6[P_2W_{18}O_{62}^{6-}]$.

B. Choice of new force field parameters

To generate a model that reproduces the bulk properties of POM-ILs and overcomes the limitations of standard force fields, one must properly account for the unique nature of these compounds. Electrostatic and van der Waals interactions play a key role in ionic liquids, with recent studies highlighting the importance of the latter, particularly the influence of short range interactions on structural organization and the resulting physicochemical properties.[50-51] Taking this into account, a significant challenge arises in molecular dynamics simulations of POM-IL systems, where charge transfer and polarizability effects are not explicitly captured by standard force fields and must be introduced *ad hoc*. Overlooking these factors in simulations can result in significant inaccuracies, such as overestimated viscosities and significantly lower diffusion coefficients. These discrepancies are largely due to the bulky nature of the ions, their close proximity, and strong, continuous interactions between them, which give rise to continuous charge polarization and, ultimately, to partial charge

transfer between anions and cations.[3,8] These limitations could potentially be addressed by employing polarizable force fields, which incorporate the distortions of the atomic electron density in an approximate manner, but at a computational cost 3–10 times larger,[52] impeding their widespread use in large and complex systems, such as POM-ILs. Furthermore, adapting a polarizable force field to such a complex system is a nontrivial task and might not guarantee improved performance. The inherent size and complexity of POM-ILs further amplifies this computational cost, making them harder to simulate compared to standard ILs.[23,53-54]

To develop parameters capable of accurately reproducing the behavior of POM-ILs, we adopted strategies that involve modifying well-defined atomic features, such as atomic charges and Lennard-Jones parameters. These adjustments allow us to incorporate polarization effects and other key interactions in both the POMs and the cations.

Scaling of atomic charges. Atomic charges receive particular attention in MD simulations of ILs, as they play a key role in electrostatic interactions and strongly influence bulk properties. A widely adopted approach involves scaling the QM-calculated values by a factor between 0.7 and 0.9 to mimic the charge transfer and polarization effects occurring in real ILs.[11,61] This approach is supported by several computational studies[30,62] in which atomic charges are derived from AIMD simulations or static QM calculations in vacuum. The reduced atomic charge values observed for ion pairs are mainly justified by the fact that the resulting net charges are consistently smaller than their formal ±1 values. Remarkably, the use of *ad hoc* scaled atomic charges in MD simulations has been shown to significantly improve the prediction of both dynamic and thermodynamic properties,[11,63-64] in agreement with experimental data such as transport properties. Importantly, this adjustment maintains consistency with thermodynamic and structural properties, providing further supporting for this approach.[3,65-66]

The protocol adopted in this work applies a charge scaling factor of 0.8 to the computed ChelpG values, as described by Canongia Lopes et al.[67] Additionally, Shannon ionic radii[68] were applied to define the atom sizes, ensuring consistency in the representation of the electrostatic environment. This combination of charge scaling, basis sets, and atom sizes provides a reasonable balance between computational efficiency and accurate modeling of POM-ILs.

It is worth noting that atomic charges can depend on molecular geometry. Although ChelpG charges often yield reliable molecular charge distributions, they may exhibit significant (even non-physical) conformational dependence.[69-70] In the case of POM-ILs, this effect is largely mitigated by the structural rigidity of the POM anion, which effectively eliminates conformational variability and, consequently, geometry-induced variations in the calculated charges.

Also, the negative charges of the POMs studied (–2 to –10) lead to stoichiometries deviating from the typical 1:1 ratio in ILs. This likely influences their behavior, particularly through strong electronic polarization and possible charge transfer between the constituent ions, resulting in effective ionic

charges that differ from their formal values. Such behavior reflects the intrinsic complexity of POM-IL systems, where electrostatic interactions (stronger than those in conventional ILs due to the highly charged POMs) may play a critical role. Accounting for this phenomenon in computational models is therefore essential to achieve more realistic simulations.[71-73]

σ and ε Lennard-Jones parameters. A well-known property of POMs is their general electron-accepting nature. The relatively low energy of their unoccupied molecular orbitals often enables electron density transfer from other molecules. While the charge scaling presented above has proven effective in many conventional ILs, it may not, on its own, fully capture all experimental observations. In such cases, further refinement, such as adjusting Lennard-Jones (LJ) parameters, can help improve the agreement between computational predictions and experimental data.[74] Rather than developing an entirely new parameter set, we introduced small adjustments to the LJ parameters to improve MD simulations while relying on standard Amber force fields and available computational resources. Our methodology builds on parameters derived from, and compared with, previous force fields for ILs such as CL&P,[37] Köddermann[1] and the General Amber Force Field (GAFF) employed by Sprenger et al.[9]

Given the limited experimental and computational data available for POM-ILs, and the absence of a well-established related computational framework, we propose adapting an existing, widely used force field with minimal modifications to preserve its general applicability.[12] Specifically, we tested small variations in the atomic σ parameter using scaling factors of 0.9 and 1.1, while initially keeping ε unmodified. Additional combinations of scaled σ and ε values were explored based on comparisons with IL-specific force fields (see the ESI). Despite these efforts, no definitive conclusions could be drawn regarding the effect of ε, primarily due to the lack of sufficient data to assess its influence on the behavior of POM-ILs.

Table 2. Atomic non-bonded σ and ε parameters of the Amber force field, and variations A, B and C analyzed. The underlined parameters are different from the original Amber force field.

Atom type	Amber		force field A		force field B		force field C	
	σ[b]	ε[b]	σ	ε	σ	ε	σ	ε
C_T	3.39967	0.457730	<u>3.05970</u>	0.457730	<u>3.05970</u>	0.457730	<u>3.05970</u>	0.457730
H_C	2.64953	0.0656888	<u>2.38458</u>	0.0656888	<u>2.38458</u>	0.0656888	<u>2.38458</u>	0.0656888
P	3.74177	0.836800						
O_P	3.17000[a]	0.897500[a]	3.17000	0.897500	<u>2.85300</u>	0.897500	<u>3.48700</u>	0.897500
H_P	1.06908[a]	0.0656888[a]						
P_P	3.74177	0.836800						
W_P	2.34000[a]	0.925000[a]						
Mo	2.71900[a]	0.234300[a]						

[a] Atomic POM parameters taken from previous works. [b] Units: σ in nm and ε in kJ mol^{-1}.

Table 2 summarizes the sets of σ and ε LJ parameters applied (variations labelled A–C) to the systems analyzed. The baseline parameters are taken from the Amber force field (also shown), including specific terms for POM atoms as defined by López et al.[41] Among the variations considered, force field A applies a 0.9 scaling factor to the σ parameters of C and H atoms in the cations. This adjustment is aimed to enhance cation mobility, accounting for their relatively small size and structural flexibility. However, it does not fully compensate for the larger size and high negative charge of the POM anions, which significantly limit their mobility (especially under a classical force field).

Force field B explores a uniform 0.9 scaling of σ for both POM and cation atoms, allowing for broader changes in interaction dynamics. Force field C incorporates the electron-accepting capacity of the POM by reducing the σ of cation atoms by 0.9 while increasing the σ of POM oxygens atoms by 1.1. Our focus on tuning the σ parameter is intentional: as a geometrical term, it can be easily adjusted to capture system-specific effects and plays a key role in modulating short-range interactions. Furthermore, σ is closely related to charge transfer and variations in effective atomic size during ion pairing. In addition, the impact of varying the atomic ε parameter was explored (see Table S1 in the ESI). Overall, these modifications did not significantly change the behavior of the system. In some cases, variations in σ and ε appeared to mutually counterbalance or resulted in overly strong interactions, occasionally introducing artifacts. For PR_4^+ cations, adjustments were limited to the carbon and hydrogen atoms of the aliphatic chains, where electron density is more easily polarizable. For POM anions, modifications were restricted to oxygen atoms (see Figure 1). These changes were intentionally minimal to preserve the general applicability of the force field across all POM-ILs under study, ensuring that the proposed modifications remain broadly relevant and transferable.

C. Results of MD simulations

Self-diffusivity (*D*). To evaluate the performance of the proposed force field parameters, we firstly focus on the transport properties of the systems. In particular, we analyze the self-diffusivity coefficient (*D*), as it is relatively straightforward to compute and provides a direct measure of the collective dynamic behavior. Other transport-related properties, such as the shear viscosity, are more computationally challenging due to convergence issues associated with the autocorrelation function of the pressure tensor.[75-77]

While experimental diffusivity data for POM-ILs are not available, viscosity values (η) have been reported. Given the inverse relationship between *D* and η described by the Stoke-Einstein equation (Eq. 4), we used viscosity data to support out analysis.

$$D = \frac{kT}{6\pi a\eta} \quad (4)$$

Due to the complex geometries of ionic liquids, accurately determining the effective radius (a) of their components Is non-trivial. As a result, we did not pursue a detailed numerical estimation of the diffusivity. Instead, we used the physical appearance and known descriptive properties of the ionic liquid to guide our interpretation of the simulation results.

The self-diffusivity coefficients for cations and anions were computed separately using the Einstein relation (Eq. 5). For a given molecule A, its diffusivity coefficient D is based on the root mean square displacement (RMSD) of its center of mass over the simulation time:

$$\frac{1}{6}\lim_{t\to\infty}\langle\|r_i(t) - r_i(0)\|^2\rangle_{i\in A} = D\cdot t \qquad (5)$$

with the factor 1/6 accounting for the degrees of freedom of a three-dimensional system.

Table 3. Self-diffusivity values (*D*) computed at 350 K for cations and anions (10^{-11} m^2s^{-1}) in all systems. The force fields applied are Amber and the variations A–C (see text and Table 1 for details). The rightmost column refers to the average self-diffusivity applying force field C to POM-ILs.

Systems	Amber		A		B		C	
	D_{Cation}	D_{Anion}	D_{Cation}	D_{Anion}	D_{Cation}	D_{Anion}	D_{Cation}	D_{Anion}
$(P_{4,4,4,10}^+)_2[W_6O_{19}^{2-}]$	0.080	0.040	0.452	0.122	0.492	0.226	0.277	0.097
$(P_{6,6,6,14}^+)_2[W_6O_{19}^{2-}]$	0.067	0.041	0.398	0.284	0.471	0.267	0.320	0.190
$(P_{6,6,6,14}^+)_3[PW_{12}O_{40}^{3-}]$	0.053	0.031	0.149	0.056	0.163	0.046	0.122	0.042
$(P_{4,4,4,16}^+)_3[PW_{12}O_{40}^{3-}]$	0.053	0.024	0.165	0.046	0.151	0.034	0.128	0.028
$(P_{6,6,6,14}^+)_6[H_2W_{12}O_{40}^{6-}]$	0.089	0.029	0.313	0.101	0.386	0.127	0.263	0.083
$(P_{6,6,6,14}^+)_{10}[H_2W_{12}O_{42}^{10-}]$	0.101	0.027	0.480	0.137	0.489	0.122	0.443	0.138
$(P_{6,6,6,14}^+)_7[PW_{11}O_{39}^{7-}]$	0.061	0.024	0.350	0.160	0.454	0.159	0.289	0.114
$(P_{4,4,4,16}^+)_7[PW_{11}O_{39}^{7-}]$	0.064	0.023	0.248	0.066	0.327	0.083	0.209	0.044
$(P_{6,6,6,14}^+)_4[W_{10}O_{32}^{4-}]$	0.040	0.018	0.153	0.059	0.185	0.078	0.133	0.052
$(P_{6,6,6,14}^+)_6[P_2Mo_{18}O_{62}^{6-}]$	0.049	0.016	0.134	0.032	0.119	0.034	0.146	0.031
$(P_{4,4,4,16}^+)_6[P_2Mo_{18}O_{62}^{6-}]$	0.103	0.018	0.190	0.022	0.195	0.022	0.158	0.018
$(P_{6,6,6,14}^+)_6[P_2W_{18}O_{62}^{6-}]$	0.070	0.017	0.151	0.033	0.184	0.041	0.175	0.037
$(P_{6,6,6,14}^+)[Cl^-]$	0.252	0.365	3.395	4.835	–	–	–	–
$(OMIM^+)[Tf_2N^-]$ [a]	0.182	0.135	1.295	0.941	1.650	1.385	–	–

[a] Calculated at 303 K for a better comparison with experimental and computational works of Sprenger et al.[9]

The systems studied are listed in Table 3, alongside two well-known reference ILs: $(P_{6,6,6,14}^+)[Cl^-]$ and $(OMIM^+)[Tf_2N]^-$ ($OMIM^+$: 1-octyl-3-methylimidazolium; Tf_2N^-: bis[(trifluoromethyl)sulfonyl]imide). The latter was included for comparison with previous studies by Sarman et al.[3] and Sprenger et al.[9,65]

Our data reveal that the classical Amber force field significantly underestimates diffusivity across all studied systems, including the reference ILs, even when applying the 0.8 scaling factor to atomic

charges. For ($OMIM^+$)[Tf_2N^-], with well-known bulk properties, the corrections introduced in force field A were essential to reproduce the experimental diffusivity of $D = 1.17 \cdot 10^{-11}$ m^2s^{-1} at 303 K for both cations and anions. The currently computed cation diffusivities, $D_{Cat} = 3.4 \cdot 10^{-11}$ for ($P_{6,6,6,14}^+$)[Cl^-] and $D_{Cat} = 1.3 \cdot 10^{-11}$ m^2s^{-1} for ($OMIM^+$)[Tf_2N^-]), are approximately one order of magnitude higher than those obtained with the original Amber force field. Unless otherwise stated, we refer to cation diffusivities as representative of the overall system diffusivity, as cations better reflect the fluidity of the ionic liquid.

In general, scaling down the σ parameter for cations only (force field A) leads to increased mobility for both ionic species, enhancing the overall dynamics of the system. Additional trends emerge across the different ILs studied. For instance, ($P_{6,6,6,14}^+$)$_{10}$[$H_2W_{12}O_{42}^{10-}$] exhibits the highest mobility with force field A, with $D = 0.480 \cdot 10^{-11}$ for the cation and $0.137 \cdot 10^{-11}$ m^2s^{-1} for the POM, in line with experimental observations (Table 1). However, the computed *D* calculated for bulkier systems such as Wells-Dawson and decatungstate salts are not satisfactory. Their measured viscosities are significantly higher than those of Keggin-based systems (>20 kPa·s), which implies lower expected diffusivities (yet our simulations fail to reflect this). Experimentally, Keggin-structured ILs behave as semi-solids, which is not reflected in our present results.

In the second test (force field B), the σ parameter for both ionic components were reduced to account for potential negative-to-positive charge transfer. Nevertheless, the resulting diffusion coefficients remain similar in magnitude to those from force field A, and the overall trends deviate from both the observations by Martinetto et al.[58] and the experimental data presented in Table 1. For example, the W_6O_{19}-based systems show higher mobilities than the paratungstate salt, contrary to experimental expectations. Likewise, Keggin-based ILs still exhibit too large *D* values within the series. It should be also noted that force field B overestimates the diffusivity of ($OMIM^+$)[Tf_2N^-]. This discrepancy may be explained by our Bader charge analysis, which reveals where minimal charge transfer in this system. Taken together, these results indicate that further refinement of the force field parameters is necessary.

Finally, considering the electron-accepting nature of POMs, force field C was tested by reducing the σ parameters of the cations and increasing those of the POM oxygens atoms by a factor 1.1. This adjustment accounts for the electron density redistribution toward the POM and, remarkably, produces ion diffusivity values (Table 3) in line with experimental trends. Among the systems tested, ($P_{6,6,6,14}^+$)$_{10}$[$H_2W_{12}O_{42}^{10-}$] again exhibits the highest mobility, establishing it as a benchmark for other POM-ILs.

It is worth pointing out that *D* remains somewhat overestimated for the Keggin-based systems. One possible explanation lies in the use of a force field originally developed for liquids, now applied to systems that exhibit semi-solid behavior. As a result, part of the observed mobility may be an artifact

generated by the model. Even so, Keggin-based ILs still show the lowest *D* values among all systems considered, preserving the correct qualitative trend.

Additional MD simulations with force field C were conducted at 373 K for two high-mobility systems, namely $(P_{6,6,6,14}^{+})_{10}[H_2W_{12}O_{42}^{10-}]$ and $(P_{6,6,6,14}^{+})_2[W_6O_{19}^{2-}]$, as well as on the less mobile $(P_{6,6,6,14}^{+})_3[PW_{12}O_{40}^{3-}]$. As expected, the paratungstate and Lindqvist-based system showed enhanced diffusivity at elevated temperature, with $D_{Cat} = 0.448 \cdot 10^{-11}$ and $D_{POM} = 0.138 \cdot 10^{-11}$ m^2s^{-1} for Lindqvist; $D_{Cat} = 0.605 \cdot 10^{-11}$ and $D_{POM} = 0.177 \cdot 10^{-11}$ m^2s^{-1} for paratungstate. In contrast, the Keggin-based system barely gained mobility ($D_{Cat} = 0.136 \cdot 10^{-11}$ and $D_{POM} = 0.045 \cdot 10^{-11}$ m^2s^{-1}), remaining highly viscous. These results are consistent with earlier findings and further supported by experimental observations.

QM analysis of the cation-anion charge transfer. One of the distinctive features of ILs is the occurrence of non-negligible electron density transfer, typically from anions to cations, resulting in net molecular charges that are lower than their formal values. To investigate whether a similar behavior occurs in POM-ILs, we performed DFT calculations on a representative MD snapshot for each system. Each snapshot contains one POM anion and the stoichiometric number of nearest-neighbor cations.

Table 4. Molecular charges obtained with Bader's QTAIM analysis, and corresponding charge transfer between (Q_{don}) the ions of the studied systems.

System	q_{CATION}^{+}	q_{ANION}^{-}	Q_{don}	q/m
$(P_{6,6,6,14}^{+})[Cl^{-}]$	0.93	–0.93	–	–
$(OMIM^{+})[Tf_2N^{-}]$	1.04	–1.05	–	–
$(P_{4,4,4,10}^{+})_2[W_6O_{19}^{2-}]$	1.12	–2.18	0.09	0.33
$(P_{6,6,6,14}^{+})_3[PW_{12}O_{40}^{3-}]$	1.14	–3.42	0.14	0.25
$(P_{6,6,6,14}^{+})_4[W_{10}O_{32}^{4-}]$	1.10	–4.38	0.10	0.40
$(P_{6,6,6,14}^{+})_6[H_2W_{12}O_{40}^{6-}]$	1.07	–6.42	0.07	0.50
$(P_{6,6,6,14}^{+})_6[P_2W_{18}O_{62}^{6-}]$	1.09	–6.55	0.09	0.33
$(P_{6,6,6,14}^{+})_7[PW_{11}O_{39}^{7-}]$	1.05	–7.34	0.05	0.64
$(P_{6,6,6,14}^{+})_{10}[H_2W_{12}O_{42}^{10-}]$	1.02	–10.21	0.02	0.83

A QTAIM Bader analysis was carried out to examine the electron density distribution. The results, summarized in Table 4, reveal a clear charge transfer from cations to the POMs, an observation finding that, at first sight, may appear counterintuitive, as it goes in opposite direction to that commonly seen in conventional ILs. However, the present analysis emphasizes that the electron-accepting nature of POMs can invert the typical charge-transfer behavior. Consequently, these findings provide a compelling explanation for the improved accuracy of our force field model, which aligns with this observed electron density redistribution.

In some of our previous studies,[78] we introduced the *q*/*m* parameter (*q*: molecular charge, *m*: number of metal centers) as an intuitive descriptor of the molecular charge density of POMs. Initially proposed to rationalize their redox behavior, *q*/*m* has also proven useful in explaining other properties, such as its basicity or its chaotropicity.[79]

In this work, we extended the use of the *q*/*m* parameter to examine POM-cation interactions in ILs. As shown in Table 4, systems exhibiting the highest charge transfer per cation (Q_{don}) correspond to those with the lowest *q*/*m*. This relationship also correlates with ion mobility: systems with higher Q_{don} generally show reduced diffusivity. For example, the Keggin-based ILs display significant charge transfer (0.14 e^- per cation) and correspondingly low mobility. These results suggest that *q*/*m* is a meaningful descriptor for understanding how electronic structure influences intermolecular interactions in POM-ILs. The QTAIM analysis thus offers a more comprehensive understanding of the charge-transfer phenomena, helping to explain the behavior captured by force field C, insights that go beyond what can be predicted using conventional electrostatic models.

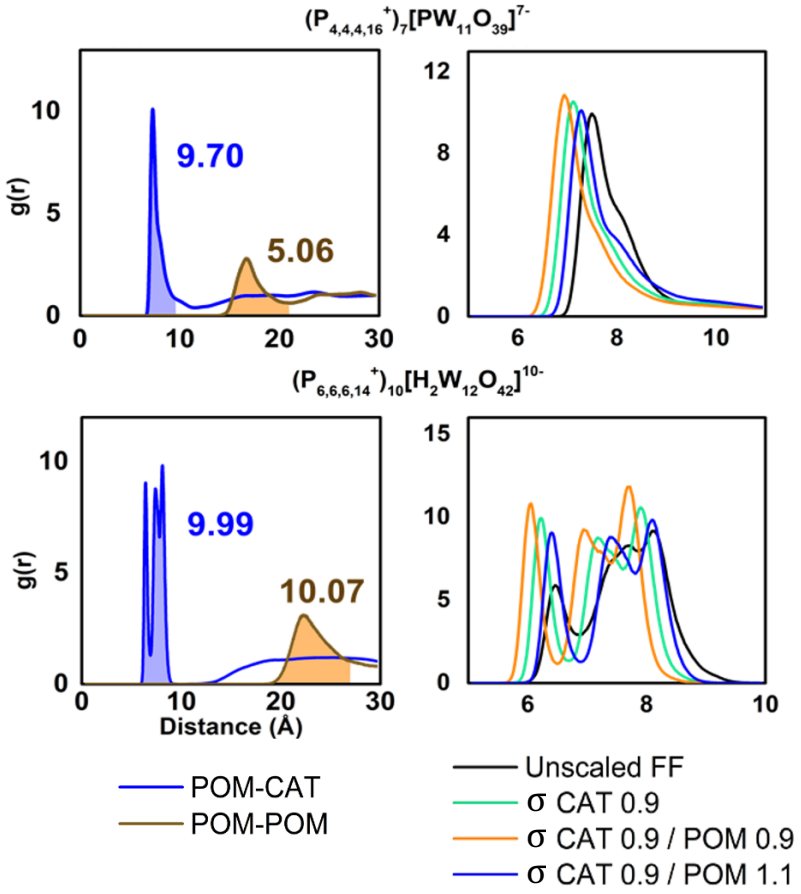

Figure 3. Comparison of systems $(P_{4,4,4,16}^+)_7[PW_{11}O_{39}^{7-}]$ (top) and $(P_{6,6,6,14}^+)_{10}[H_2W_{12}O_{42}^{10-}]$ (bottom). Left plots show cation-POM (blue line) and POM–POM (orange line) RDFs obtained with Force Field C, and integration values of the shaded peaks. The numbers correspond to integration of the shaded area, that is, the number of molecules found within the corresponding peak. Right plots show cation–POM RDFs for the various force fields tested.

POM environment. One approach to assess the impact of atomic parameter scaling on structural organization is through analysis of the POM–cation radial distribution functions (RDFs). In most cases, the RDFs are nearly identical across the four tested force fields (Figure S1 in the ESI), suggesting that the applied modifications do not substantially perturb POM-cation interactions. Exceptions are observed for systems with highly charged POMs, namely [$PW_{11}O_{39}^{7-}$] and [$H_2W_{12}O_{42}^{10-}$] (left side of Figure 3), suggesting that in these cases, the local environment around the POM is more sensitive to parameter changes.

A more detailed analysis of force field C provides deeper insight into the spatial distribution of species within the simulation box. Comparison of POM-cation and POM-POM RDFs (right side Figure 3) reveals a prominent first peak in the POM-cation RDF, indicating a high local concentration of cations around each POM, often exceeding the expected stoichiometry. This finding implies that some cations are tightly bound to individual POMs, while others are shared among neighboring POMs. These shared cations contribute collectively to the RDF, promoting a moderate level of structural ordering throughout the system. Notably, POMs that tend to attract a larger number of cations are typically those with greater surface area or stronger electrostatic potential, reinforcing the role of POM-specific features in guiding local ion organization.

Among the systems studied, $(P_{6,6,6,14}^{+})_{10}[H_2W_{12}O_{42}^{10-}]$ is the only one that presents several (three) sharp and well-resolved peaks in the POM-cation RDF, as shown in Figures S1 and S2 (see ESI, force field C). This behavior reflects the strong electrostatic attraction between cations and the highly charged POM (q = –10). The presence of three distinct peaks is related to the low sphericity of the POM and, hence, to the different distances at which the cations are attached with respect to the center of the POM. A similar, though less pronounced, effect is observed in other non-spherical POMs, such as $W_{10}O_{32}$ and $P_2W_{18}O_{62}$, which display RDF shoulders rather than distinct peaks. In these cases, explaining the appearance of only a single dominant peak.

Inspection of the POM-POM RDFs (Figure 3, superimposed to POM-cation RDFs) systematically shows a broad peak at longer distances, whose position and width vary across systems. In some cases, such as [$W_6O_{19}^{2-}$] and [$PW_{12}O_{40}^{3-}$], POM units are found at well-defined separations, suggesting a degree of rigidity or local ordering within the fluid. The average POM-POM distance, defined by the position of the RDF peak, depends both on the specific POM geometry and on the arrangement of shared cations (see Figure S2). Notably, the [$H_2W_{12}O_{42}^{10-}$] system exhibits the largest average separation between POM units. This can be explained by the presence of two distinct cation layers between neighboring POMs (Figure 4B), which increase their mutual separation compared to the $(P_{4,4,4,16}^{+})_7[PW_{11}O_{39}^{7-}]$ system, for example, in which cations are more shared between neighboring POMs (Figure 4A).

The resulting POM–POM RDF is reminiscent of assembly patterns observed in other POM-based studies, where cations mediate the association of multiple POM units. However, in the present POM-IL systems, this behavior should not be interpreted as a distinct "aggregation phenomenon". Instead, it reflects the supramolecular organization intrinsic to the ionic liquid phase, in which both POMs and cations contribute collectively to the bulk structure. In line with the work of Solé-Daura et al.,[80] an abundance of cations can mitigate electrostatic repulsion between highly charged anions, effectively promoting cation-mediated bridging between POMs. It is also important to emphasize the importance of ion-pairing interactions reported in that same study, an aspect we will revisit later in this work to further highlight its significance in the context of POM-IL behavior.

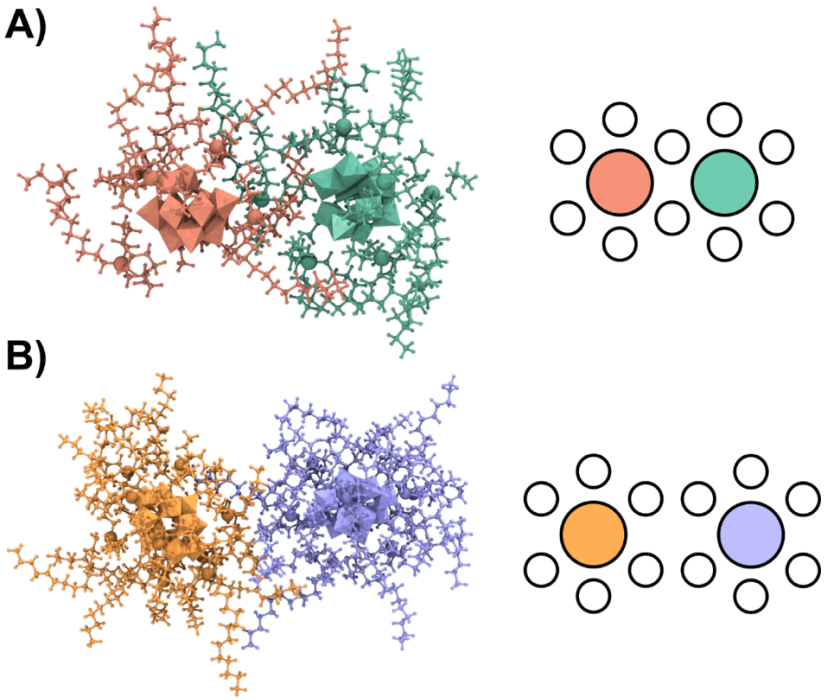

Figure 4. Selected MD snapshots (left) and simplified representations (right, with cations as empty circles) of two POM-ILs featuring different aggregation modes. A) $(P_{4,4,4,16}^{+})_7[PW_{11}O_{39}^{7-}]$ system, in which part of the cations represented are shared by the two POM units; B) $(P_{6,6,6,14}^{+})_{10}[H_2W_{12}O_{42}^{10-}]$ system, where each POM unit carry its own cation shell. Coloring helps identifying the POM-cations.

Collective system behavior. In addition to the structural features discussed above, certain cations, such as $P_{6,6,6,14}^{+}$, with its extended alkyl chains, can further influence the microstructure by altering both local packing and overall dynamics. In this section we delve into how these structural characteristics correlate with diffusivity in the simulations, providing a more comprehensive understanding of POM-ILs behavior.

Following the structural analysis with force field C, we compared systems sharing the same anion to isolate the effects of varying the cation. POM-ILs containing $P_{6,6,6,14}^{+}$ generally exhibit slightly higher mobility than their counterparts with shorter alkyl chains, resulting in materials with enhanced

macroscopic fluidity. Longer alkyl chains confer greater conformational freedom to the cation, increasing overall mobility of the ionic ensemble (Figure S3 in the ESI). The enhanced cation mobility also leads to higher anion diffusivity. The influence of the cation is particularly evident in systems containing [$W_6O_{19}^{2-}$] and [$PW_{12}O_{40}^{3-}$], whereas in Dawson-type anions the effect appears less pronounced (Table 3). These observations underscore the inherent complexity of POM-IL systems, where multiple independent factors contribute to the observed macroscopic properties. For clarity, the subsequent discussion focuses primarily on systems incorporating $P_{6,6,6,14}^{+}$.

Table 5. Average cation-anion interaction energies (E_{int}) calculated from MD simulations in kcal mol^{-1}, scaled by the number of interacting cations identified (via RDF Integration).

System	E_{int}
$(P_{4,4,4,16}^{+})_2[W_6O_{19}^{2-}]$	–13.24
$(P_{6,6,6,14}^{+})_2[W_6O_{19}^{2-}]$	–14.85
$(P_{6,6,6,14}^{+})_3[PW_{12}O_{40}^{3-}]$	–18.96
$(P_{4,4,4,16}^{+})_3[PW_{12}O_{40}^{3-}]$	–16.76
$(P_{6,6,6,14}^{+})_6[H_2W_{12}O_{40}^{6-}]$	–27.54
$(P_{6,6,6,14}^{+})_{10}[H_2W_{12}O_{42}^{10-}]$	–32.78
$(P_{6,6,6,14}^{+})_7[PW_{11}O_{39}^{7-}]$	–29.41
$(P_{4,4,4,16}^{+})_7[PW_{11}O_{39}^{7-}]$	–23.69
$(P_{6,6,6,14}^{+})_4[W_{10}O_{32}^{4-}]$	–18.45
$(P_{6,6,6,14}^{+})_6[P_2W_{18}O_{62}^{6-}]$	–19.13
$(P_{4,4,4,16}^{+})_6[P_2W_{18}O_{62}^{6-}]$	–18.30
$(P_{6,6,6,14}^{+})_6[P_2W_{18}O_{62}^{6-}]$	–20.21
$(P_{6,6,6,14}^{+})[Cl^{-}]$	–5.57

The size of the POM also affects the properties of the system. Bulky anions, such as [$P_2Mo_{18}O_{62}^{6-}$], have significantly reduced freedom of movement compared to smaller POMs. This limitation weakens the effect of cation substitution on the overall dynamics. In addition to the size, the molecular charge of the POM influences the dynamics of the system. Interestingly, our data show that the most negatively charged POMs, such as the paratungstate (q = –10), display the highest diffusion coefficients. While one might expect stronger electrostatic interactions to hinder mobility, the results suggest otherwise. To understand this counterintuitive observation, we calculated the average POM-cation interaction energies (E_{int}) for each system along the simulation. These values were normalized by the number of interacting cations, as determined by integration of the POM-cation RDF, to allow for direct comparison across the series (Table 5). This normalization provides a consistent measure of the cation contribution to total pairwise interactions. A clear trend emerges when comparing E_{int} with

diffusivity (D) values (Figure 5): systems exhibiting stronger (more negative) average POM-cation interactions tend to display greater mobility. Furthermore, the overall system mobility (D_{System}, black dots) closely follows the trend of cation diffusivity (D_{Cat}, red circles), reinforcing the dominant role of cations in governing bulk dynamics.

Notably, two systems deviate from the main trend: $(P_{4,4,4,10}^{+})_2[W_6O_{19}^{2-}]$ and $(P_{6,6,6,14}^{+})_2[W_6O_{19}^{2-}]$ exhibit relatively high mobilities (D_{System} = $0.217 \cdot 10^{-11}$ and $0.277 \cdot 10^{-11}$ m^2s^{-1}, respectively), ranking among the most fluid systems studied. These deviations highlight the importance of considering not only pairwise interactions, but also the spatial organization and packing of ions in determining macroscopic transport properties.

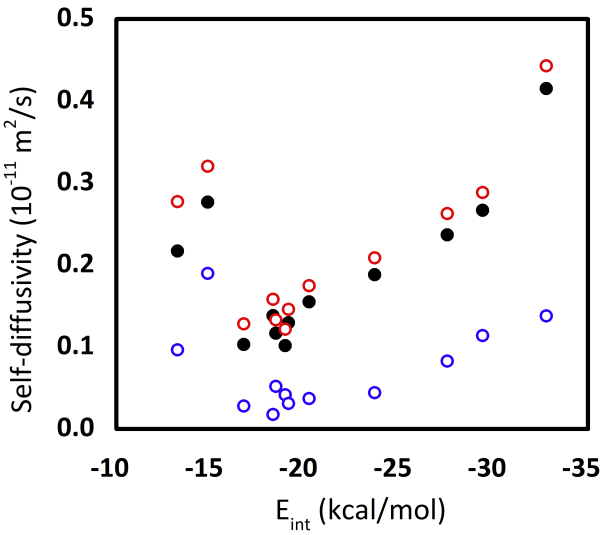

Figure 5. Representation of the system self-diffusivity vs the cation-anion interaction energy (listed in Table 3) for the ILs herein studied. Partial values for cation and anion are represented by red and blue circles, respectively, and total system values by black dots. Total and cation diffusivities are very similar.

The strength of the POM-cation interactions, which depends on their mutual distance, leads some cations, particularly those closest to the POM, to become tightly bound. This strong association reduces their individual mobility but promotes the collective motion of POM-cation aggregates. In contrast, cations located farther away, which are more loosely associated or shared between neighboring POMs, may appear more mobile. However, their ability to transiently coordinate with multiple POMs or introduce steric hindrance can ultimately restrict the overall dynamics of the system. This spatial arrangement suggests a supramolecular organization in which tightly bound cations move in concert with their corresponding POM, while the more distant, seemingly freer cations actually limit collective motion. This behavior is clearly illustrated when comparing $(P_{6,6,6,14}^{+})_{10}[H_2W_{12}O_{42}^{10-}]$ and $(P_{6,6,6,14}^{+})_6[P_2Mo_{18}O_{62}^{6-}]$. Although the RDFs of both systems indicate 9 and 10 nearby cations,

respectively, in the former case the cations are more tightly bound to the POM, while in the latter they are more diffusely distributed or located at greater distances, as observed in Figure 6 (and in Figure S4 in the ESI).

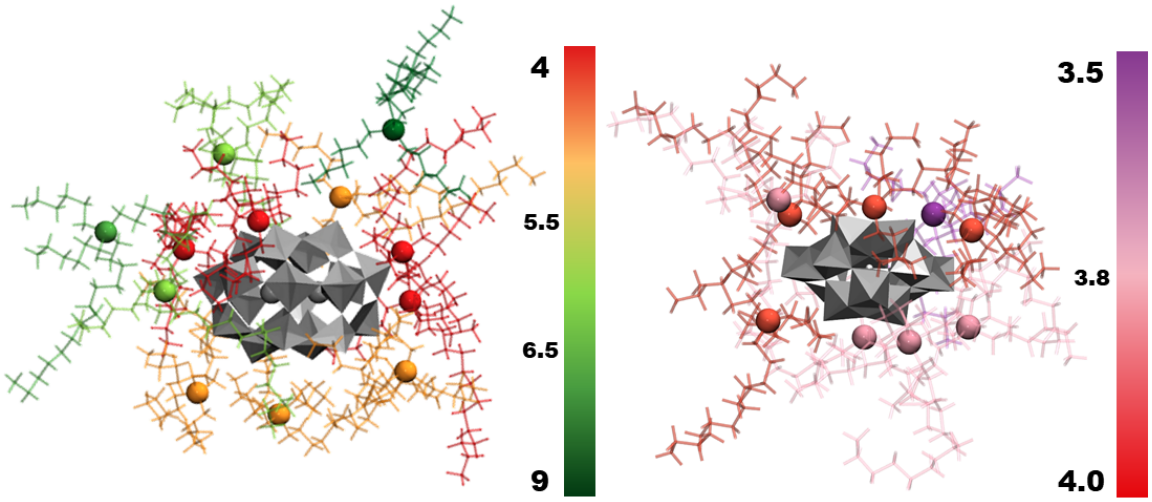

Figure 6. Cations interacting in $(P_{6,6,6,14}^{+})_6[P_2Mo_{18}O_{62}^{6-}]$ on left and $(P_{6,6,6,14}^{+})_{10}[H_2W_{12}O_{42}^{10-}]$ on the right. The distance units are in Å from the POM surface to de P atom.

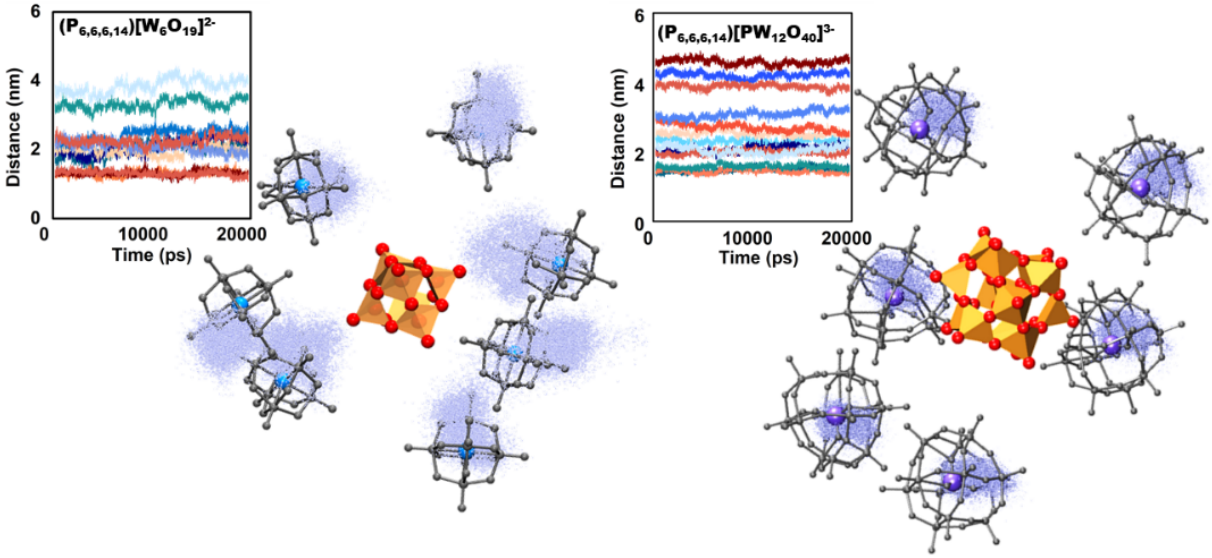

Figure 7. Evolution of the POM-POM distance along the simulation with respect to a reference anion and representation of the nearest POM positions during the simulation, showing the translation of the central oxo of the POM for $(P_{6,6,6,14}^{+})_2[W_6O_{19}^{2-}]$ (left) and the phosphorus atom of the POM for $(P_{6,6,6,14}^{+})_2[PW_{12}O_{40}^{3-}]$ (right).

These different arrangements explain the higher diffusivity observed in highly charged systems. Despite stronger POM-cation interactions, the formation of compact, mobile aggregates contributes to enhanced overall transport. Consequently, POM mobility in POM-ILs is primarily governed by

localized fluctuations and short-range motion, rather than long-range translation, contrasting with simpler ionic liquids, such as $(P_{6,6,6,14}^{+})[Cl^{-}]$, where the anion exhibits significantly greater translational freedom. At the simulated temperature (350 K), POMs in POM-ILs predominantly fluctuate and reorient within a large, ordered network (Figure 7 and Figure S5 in the ESI). This behavior is also reflected in the stability of inter-anion distances over the course of the simulation, as shown in Figure 8A.

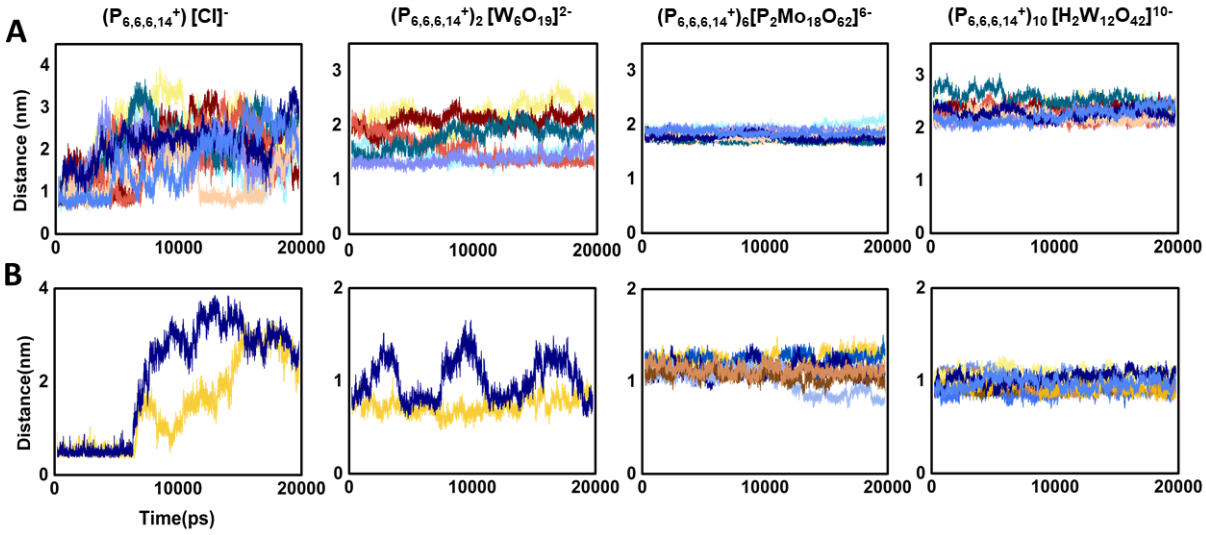

Figure 8. (A) Anion-anion distances for 10 random pairs monitored vs the simulation time (in ps) for systems of different mobility, and (B) evolution of the anion-cation distance vs the simulation time. In this case, the number of cations nearest to the anion, determined by stoichiometry, is tracked over time.

Motivated by these observations, we extended the Coulombic interaction cutoff from 1.4 nm to 3.0 nm to account for the potential influence of long-range electrostatics in systems comprising highly charged POM networks. Two of the most mobile systems, namely $(P_{6,6,6,14}^{+})_{10}[H_2W_{12}O_{42}^{10-}]$ and $(P_{6,6,6,14}^{+})_2[W_6O_{19}^{2-}]$, were selected for this analysis. Diffusivities obtained with the extended cutoff (3.0 nm), guided by the decay of point-charge approximations for POM–POM interactions, showed minimal variation compared to the original cutoff. For paratungstate, $D_{Cat} = 0.468 \cdot 10^{-11}$ and $D_{POM} = 0.151 \cdot 10^{-11}$ m^2s^{-1}, while the Lindqvist system yielded $D_{Cat} = 0.397 \cdot 10^{-11}$ and $D_{POM} = 0.224 \cdot 10^{-11}$ m^2s^{-1}. These differ from the 1.4 nm values by only 0.02–0.06 units, within typical simulation uncertainties, yet the computational cost doubled. This suggest that a 3.0 nm cutoff offers limited benefit mobility predictions in these systems.

Focusing on the fluidity, POM-ILs containing $[W_6O_{19}^{2-}]$ deviate from the general charge-based trend. Despite bearing the lowest anionic charge (q = –2), their compact size enables higher mobility, offsetting the absence of aggregation effects. A closer evaluation of the local structure (Figure 8)

confirms that while most POM-ILs display cohesive ion arrangements, $(P_{6,6,6,14}^{+})_2[W_6O_{19}^{2-}]$ displays a looser, more dynamic behavior.

As discussed thoughout this work, POM-ILs differ fundamentally from conventional ILs in both structural and dynamic regimes. Strong ion pairing leads to highly ordered phases, where POMs primarily undergo localized fluctuations rather than long-range diffusion. Figure 8 (and Figure S6 in the ESI) illustrates the contrasting behavior of a conventional IL and three representative POM-IL systems. Although both Dawson- and paratungstate-based systems exhibit aggregation, they yield opposite macroscopic properties. In the Dawson system, the large anion size limits mobility and results in higher viscosity, even with moderately mobile cations. By contrast, paratungstate retains strong cation bingind while maintaining high anion-anion mobility, contributing to overall fluidity.

To further explore this behavior, we tracked the time evolution of the two most mobile systems: $(P_{6,6,6,14}^{+})_{10}[H_2W_{12}O_{42}^{10-}]$ and $(P_{6,6,6,14}^{+})_2[W_6O_{19}^{2-}]$. Their trajectories (see Figure 9) confirm the supramolecular nature of POM-cation organization. In the Lindqvist system, random ion motion dominates, while the paratungstate exhibits a more collective dynamic behavior, where the POM moves together with a tightly associated cation shell. This contrasts with the rigid behavior seen in $(P_{6,6,6,14}^{+})_3[PW_{12}O_{40}^{3-}]$, where both cations and POMs remain largely immobilized, in agreement with experimental observations. For comparison, Figures S7 in the ESI shows the behaviour for other POM-ILs, and Figure S8 for the classical IL $(P_{6,6,6,14}^{+})[Cl^{-}]$, with very scattered clouds of points for both components of the salt.

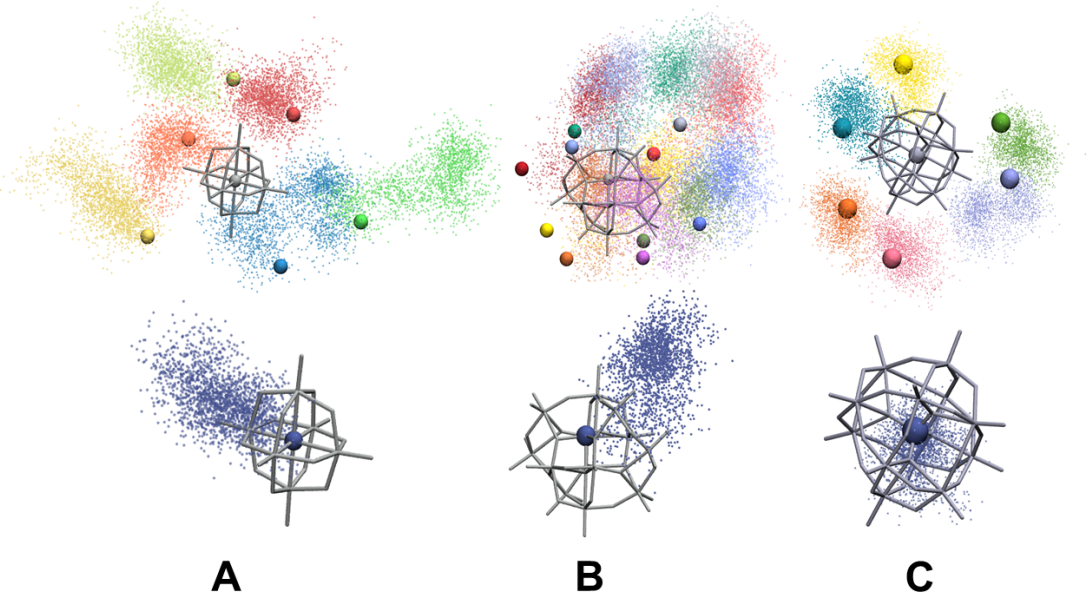

Figure 9. Graphical representation of cation and POM movement during the simulation for the following systems: (A) $(P_{6,6,6,14}^{+})_2[W_6O_{19}^{2-}]$, (B) $(P_{6,6,6,14}^{+})_{10}[H_2W_{12}O_{42}^{10-}]$ and (C) $(P_{6,6,6,14}^{+})_3[PW_{12}O_{40}^{3-}]$. The movement is depicted by the positions adopted by the P atoms (cations) and the O, H, and P atoms (POMs) respectively throughout the simulation.

Overall, these simulations show that POM-ILs exhibit notably different fundamental dynamics and microstructures compared to conventional ionic liquids. Their large anionic units and strong ion pairing create a complex interplay between localized and collective motions, which in turn define their distinctive transport and rheological properties. At the same time, our findings emphasize the importance of carefully tuning non-bonded force field parameters to capture the distinctive behavior of POM-ILs. Although only minor adjustments were made here, they significantly improved the predictive capability of the simulations. Given the limited number of studies on POM-ILs to date, the present findings may serve as a methodological reference and provide basis for future developments in molecular dynamics modeling of these complex systems.

CONCLUSIONS

This work presents the first computational analysis of polyoxometalate-based ionic liquids (POM-ILs), combining classical molecular dynamics simulations with tailored force fields, and quantum mechanical calculations. The results of the simulations are validated against published and new experimental data to assess the accuracy of the predicted trends.

The calculated results demonstrate that the commonly used atomic charge scaling factor of 0.8 is necessary but insufficient to capture the behavior of POM-ILs accurately. Due to the strong polarizability and electron-accepting character of POM anions, additional adjustments of the Lennard-Jones (LJ) parameters are required. Specifically, reducing the σ parameter for cations and increasing σ for POM oxygen atoms yields a force field that better reproduces the experimental trends of diffusivity across multiple POM-IL systems. This approach offers a practical and transferable alternative to standard force fields, that is, those developed for conventional ILs. In addition, this parametrization is consistent with the (initially) counterintuitive cation-to-POM charge transfer revealed by Bader population analysis, underscoring the importance of both charge scaling and LJ tuning in modeling the dynamics of POM-ILs. Our findings also underline the relevance of molecular charge density and POM charge as key predictors of the bulk behavior. Unlike conventional ILs (behaving as independent ions) POM-ILs exhibit a distinctive supramolecular ordering in which each POM unit and its closest cations move *en bloc*, a fact that allows for certain mobility despite the strong anion-cation electrostatic interactions. This motion observed as outcome of MD simulations on POM-ILs, different from that of conventional simpler ionic liquids, reveals unique structural and dynamic features.

Overall, this study represents a significant step towards the understanding and the modeling of POM-ILs at the theoretical level, offering insights that may guide interpretation of experimental data and future development in this field and aid practical applications.

CONFLICTS OF INTEREST

There are no conflicts of interest.

DATA AVAILABILITY

The data supporting this article (syntheses and additional graphs) have been included as part of the Supplementary Information.

ACKNOWLEDGEMENTS

This work was supported by the Generalitat de Catalunya (project 2021SGR0011)] and by the Spanish Government (grant PID2023-149905NB-I00, funded by MCIN/AEI/10.13039/501100011033). N.Z. would like to thank the University of Versailles Saint-Quentin en Yvelines and the Charmmmat labex (ANR-11-LABX-0039) for funding his thesis work. This study results from an international collaboration supported by IRN-CNRS 2019-2023. We also thank Dr. Salomé Basset and Dr. Yohan Martinetto, from Institut Lavoisier of Versailles, and Dr. Jelena Jeftic, from ISCR in Rennes, France, for their help in the experimental work.

REFERENCES

[1] Köddermann, T.; Paschek, D.; Ludwig, R. Molecular Dynamic Simulations of Ionic Liquids: A Reliable Description of Structure, Thermodynamics and Dynamics. *ChemPhysChem* **2007**, *8* (17), 2464-2470.

[2] Maginn, E. J. Atomistic Simulation of the Thermodynamic and Transport Properties of Ionic Liquids. *Acc. Chem. Res.* **2007**, *40* (11), 1200-1207.

[3] Sarman, S.; Wang, Y.-L.; Rohlmann, P.; Glavatskih, S.; Laaksonen, A. Rheology of phosphonium ionic liquids: a molecular dynamics and experimental study. *Phys. Chem. Chem. Phys.* **2018**, *20* (15), 10193-10203.

[4] Wang, Y.; Jiang, W.; Yan, T.; Voth, G. A. Understanding Ionic Liquids through Atomistic and Coarse-Grained Molecular Dynamics Simulations. *Acc. Chem. Res.* **2007**, *40* (11), 1193-1199.

[5] Krekeler, C.; Dommert, F.; Schmidt, J.; Zhao, Y. Y.; Holm, C.; Berger, R.; Delle Site, L. Electrostatic properties of liquid 1,3-dimethylimidazolium chloride: role of local polarization and effect of the bulk. *Phys. Chem. Chem. Phys.* **2010**, *12* (8), 1817-1821.

[6] Margulis, C. J.; Stern, H. A.; Berne, B. J. Computer Simulation of a "Green Chemistry" Room-Temperature Ionic Solvent. *J. Phys. Chem. B* **2002**, *106* (46), 12017-12021.

[7] Endres, F.; Zein El Abedin, S. Air and water stable ionic liquids in physical chemistry. *Phys. Chem. Chem. Phys.* **2006**, *8* (18), 2101-2116.

[8] Schröder, C.; Lyons, A.; Rick, S. W. Polarizable MD simulations of ionic liquids: How does additional charge transfer change the dynamics? *Phys. Chem. Chem. Phys.* **2020**, *22* (2), 467-477.

[9] Sprenger, K. G.; Jaeger, V. W.; Pfaendtner, J. The General AMBER Force Field (GAFF) Can Accurately Predict Thermodynamic and Transport Properties of Many Ionic Liquids. *J. Phys. Chem. B* **2015**, *119* (18), 5882-5895.

[10] Maginn, E. J. Molecular simulation of ionic liquids: current status and future opportunities. *J. Phys.: Condens. Matter* **2009**, *21* (37), 373101.

[11] Barbosa, G. D.; Liu, X.; O'Harra, K. E.; Bara, J. E.; Turner, C. H. Charge scaling parameter evaluation for multivalent ionic liquids with fixed point charge force fields. *Journal of Ionic Liquids* **2022**, *2* (1), 100020.

[12] Wang, H.; Li, B. Recent Advances on the Functionalities of Polyoxometalate-Based Ionic Liquids. *Molecules* **2024**, *29* (13), 3216.

[13] Martinetto, Y.; Pegot, B.; Roch- Marchal, C.; Cottyn Boitte, B.; Haouas, M.; Camerel, F.; Morineau, D.; Floquet, S. Application of a new polyoxometalate-based ionic liquids in "green" catalytic oxidation. In Journée de l'École Doctorale Molécules, Matériaux, Instrumentation et Biosystèmes (2MIB), Evry, France; 2019.

[14] Martinetto, Y.; Basset, S.; Pégot, B.; Roch-Marchal, C.; Camerel, F.; Jeftic, J.; Cottyn-Boitte, B.; Magnier, E.; Floquet, S. Synthesis, Physical Properties and Application of a Series of New Polyoxometalate-Based Ionic Liquids. *Molecules* **2021**, *26* (2), 496

[15] Martinetto, Y.; Pégot, B.; Roch-Marchal, C.; Haouas, M.; Cottyn-Boitte, B.; Camerel, F.; Jeftic, J.; Morineau, D.; Magnier, E.; Floquet, S. A decatungstate-based ionic liquid exhibiting a very low dielectric constant suitable for acting as a solvent and a catalyst for the oxidation of organic substrates. *New J. Chem.* **2021**, *45* (22), 9751-9755.

[16] Martinetto, Y.; Pégot, B.; Roch-Marchal, C.; Cottyn-Boitte, B.; Floquet, S. Designing Functional Polyoxometalate-Based Ionic Liquid Crystals and Ionic Liquids. *Eur. J. Inorg. Chem.* **2020**, *2020* (3), 228-247.

[17] Cruz, H.; Pinto, A. L.; Lima, J. C.; Branco, L. C.; Gago, S. Application of polyoxometalate-ionic liquids (POM-ILs) in dye-sensitized solar cells (DSSCs). *Materials Letters: X* **2020**, *6*, 100033.

[18] Li, J.; Ma, J.; Wei, C.; Zheng, Z.; Han, Y.; Wang, H.; Wang, X.; Hu, C. Polyoxometalate-based ionic liquids: efficient reversible phase transformation-type catalysts for thiolation of alcohols to construct C–S bonds. *Dalton Trans.* **2024**, *53* (10), 4492-4500.

[19] Werner, I.; Griebel, J.; Masip-Sánchez, A.; López, X.; Załęski, K.; Kozłowski, P.; Kahnt, A.; Boerner, M.; Warneke, Z.; Warneke, J.; et al. Hybrid Molecular Magnets with Lanthanide- and Countercation-Mediated Interfacial Electron Transfer between Phthalocyanine and Polyoxovanadate. *Inorg. Chem.* **2023**, *62* (9), 3761-3775.

[20] Izzet, G.; Abécassis, B.; Brouri, D.; Piot, M.; Matt, B.; Serapian, S. A.; Bo, C.; Proust, A. Hierarchical Self-Assembly of Polyoxometalate-Based Hybrids Driven by Metal Coordination and Electrostatic Interactions: From Discrete Supramolecular Species to Dense Monodisperse Nanoparticles. *J. Am. Chem. Soc.* **2016**, *138* (15), 5093-5099.

[21] Song, Y.-F.; Tsunashima, R. Recent advances on polyoxometalate-based molecular and composite materials. *Chem. Soc. Rev.* **2012**, *41* (22), 7384-7402.

[22] Floquet, S.; Terazzi, E.; Hijazi, A.; Guénée, L.; Piguet, C.; Cadot, E. Evidence of ionic liquid crystal properties for a DODA+ salt of the keplerate [Mo132O372(CH3COO)30(H2O)72]42−. *New J. Chem.* **2012**, *36* (4), 865-868.

[23] Watfa, N.; Floquet, S.; Terazzi, E.; Haouas, M.; Salomon, W.; Korenev, V. S.; Taulelle, F.; Guénée, L.; Hijazi, A.; Naoufal, D.; et al. Synthesis, characterization, and tuning of the liquid crystal properties

of ionic materials based on the cyclic polyoxothiometalate $[\{Mo_4O_4S_4(H_2O)_3(OH)_2\}_2(P_8W_{48}O_{184})]^{36-}$. *Soft Matter* **2015**, *11* (6), 1087-1099.

[24] Long, D.-L.; Tsunashima, R.; Cronin, L. Polyoxometalates: Building Blocks for Functional Nanoscale Systems. *Angew. Chem., Int. Ed.* **2010**, *49* (10), 1736-1758.

[25] López, X.; Carbó, J. J.; Bo, C.; Poblet, J. M. Structure, properties and reactivity of polyoxometalates: a theoretical perspective. *Chem. Soc. Rev.* **2012**, *41* (22), 7537-7571.

[26] Zeaiter, N.; Martinetto, Y.; Cézard, L.; Haouas, M.; Roch-Marchal, C.; Pégot, B.; Floquet, S.; Cottyn-Boitte, B. Decatungstate-Based Ionic Liquid Highly Active Under Mild Conditions for Upgrading Recalcitrant Humins from Biorefineries. *Inorg. Chem.* **2025**, *64* (11), 5495-5504.

[27] Misra, A.; Franco Castillo, I.; Müller, D. P.; González, C.; Eyssautier-Chuine, S.; Ziegler, A.; de la Fuente, J. M.; Mitchell, S. G.; Streb, C. Polyoxometalate-Ionic Liquids (POM-ILs) as Anticorrosion and Antibacterial Coatings for Natural Stones. *Angew. Chem., Int. Ed.* **2018**, *57* (45), 14926-14931.

[28] Nunes, M.; García-Orduña, P.; Atrián-Blasco, E.; Costa Vieira, J.; Costa, A. P.; Cabral Amaral, M. E.; Claro, A.; Ferreira, T.; Mitchell, S. G. Polyoxometalate-Ionic Liquids for Mitigating the Effects of Iron Gall Ink Corrosion on Cellulosic Supports. *ACS Omega* **2024**, *9* (34), 36609-36621.

[29] Mozaffari, F. Molecular dynamics simulations of the structure and dynamics in mixtures of ionic liquids and alcohols. *Phys. Chem. Chem. Phys.* **2025**, *27* (7), 3755-3772.

[30] Zhang, Y.; Maginn, E. J. A Simple AIMD Approach to Derive Atomic Charges for Condensed Phase Simulation of Ionic Liquids. *J. Phys. Chem. B* **2012**, *116* (33), 10036-10048.

[31] Gao, Y.; Choudhari, M.; Such, G. K.; Ritchie, C. Polyoxometalates as chemically and structurally versatile components in self-assembled materials. *Chem. Sci.* **2022**, *13* (9), 2510-2527.

[32] Misra, A.; Kozma, K.; Streb, C.; Nyman, M. Beyond Charge Balance: Counter-Cations in Polyoxometalate Chemistry. *Angew. Chem., Int. Ed.* **2020**, *59* (2), 596-612.

[33] Marekha, B. A.; Kalugin, O. N.; Idrissi, A. Non-covalent interactions in ionic liquid ion pairs and ion pair dimers: a quantum chemical calculation analysis. *Phys. Chem. Chem. Phys.* **2015**, *17* (26), 16846-16857.

[34] Jorgensen, W. L.; Maxwell, D. S.; Tirado-Rives, J. Development and Testing of the OPLS All-Atom Force Field on Conformational Energetics and Properties of Organic Liquids. *J. Am. Chem. Soc.* **1996**, *118* (45), 11225-11236.

[35] Vanommeslaeghe, K.; Hatcher, E.; Acharya, C.; Kundu, S.; Zhong, S.; Shim, J.; Darian, E.; Guvench, O.; Lopes, P.; Vorobyov, I.; et al. CHARMM general force field: A force field for drug-like molecules compatible with the CHARMM all-atom additive biological force fields. *J. Comput. Chem.* **2010**, *31* (4), 671-690.

[36] AMBER 2018, Case, D. A.; Ben-Shalom, I. Y.; Brozell, S. R.; Cerutti, D. S.; Cheatham, T. E.; Cruzeiro, V. W. D.; Darden, T. A.; Duke, R. E.; Ghoreishi, D.; Gilson, M. K.; et al. University of California, San Francisco, 2018.

[37] Canongia Lopes, J. N.; Pádua, A. A. H. CL&P: A generic and systematic force field for ionic liquids modeling. *Theor. Chem. Acc.* **2012**, *131* (3), 1129.

[38] Frömbgen, T.; Canongia Lopes, J. N.; Kirchner, B.; Shimizu, K. Unraveling the Morphology of [CnC1Im]Cl Ionic Liquids Combining Cluster and Aggregation Analyses. *J. Phys. Chem. B* **2024**, *128* (16), 3937-3945.

[39] Klajmon, M.; Červinka, C. Does Explicit Polarizability Improve Simulations of Phase Behavior of Ionic Liquids? *J. Chem. Theory Comput.* **2021**, *17* (10), 6225-6239.

[40] Philippi, F.; Goloviznina, K.; Gong, Z.; Gehrke, S.; Kirchner, B.; Pádua, A. A. H.; Hunt, P. A. Charge transfer and polarisability in ionic liquids: a case study. *Phys. Chem. Chem. Phys.* **2022**, *24* (5), 3144-3162.

[41] López, X.; Nieto-Draghi, C.; Bo, C.; Avalos, J. B.; Poblet, J. M. Polyoxometalates in Solution: Molecular Dynamics Simulations on the α-$PW_{12}O_{40}^{3-}$ Keggin Anion in Aqueous Media. *J. Phys. Chem. A* **2005**, *109* (6), 1216-1222.

[42] Gaussian 16, Revision A.03, Frisch, M. J.; Trucks, G. W.; Schlegel, H. B.; Scuseria, G. E.; Robb, M. A.; Cheeseman, J. R.; Scalmani, G.; Barone, V.; Petersson, G. A.; Nakatsuji, H.; et al. Gaussian, Inc., Wallingford, CT, 2016.

[43] Becke, A. D. Density-functional thermochemistry. III. The role of exact exchange. *J. Chem. Phys.* **1993**, *98* (7), 5648-5652.

[44] Becke, A. D. Density-functional exchange-energy approximation with correct asymptotic behavior. *Phys. Rev. A* **1988**, *38* (6), 3098-3100.

[45] Hay, P. J.; Wadt, W. R. Ab initio effective core potentials for molecular calculations. Potentials for the transition metal atoms Sc to Hg. *J. Chem. Phys.* **1985**, *82* (1), 270-283.

[46] Wadt, W. R.; Hay, P. J. Ab initio effective core potentials for molecular calculations. Potentials for main group elements Na to Bi. *J. Chem. Phys.* **1985**, *82* (1), 284-298.

[47] Grimme, S.; Ehrlich, S.; Goerigk, L. Effect of the damping function in dispersion corrected density functional theory. *J. Comput. Chem.* **2011**, *32* (7), 1456-1465.

[48] Mennucci, B.; Tomasi, J.; Cammi, R.; Cheeseman, J. R.; Frisch, M. J.; Devlin, F. J.; Gabriel, S.; Stephens, P. J. Polarizable Continuum Model (PCM) Calculations of Solvent Effects on Optical Rotations of Chiral Molecules. *J. Phys. Chem. A* **2002**, *106* (25), 6102-6113.

[49] Lu, T.; Chen, F. Multiwfn: A multifunctional wavefunction analyzer. *J. Comput. Chem.* **2012**, *33* (5), 580-592.

[50] GROMACS 2019.3 Manual, Lindahl, E.; Abraham, M. J.; Hess, B.; van der Spoel, D. Zenodo, 2019. 10.5281/zenodo.3243834.

[51] Perera, L.; Essmann, U.; Berkowitz, M. L. Effect of the treatment of long-range forces on the dynamics of ions in aqueous solutions. *J. Chem. Phys.* **1995**, *102* (1), 450-456.

[52] Nosé, S. An extension of the canonical ensemble molecular dynamics method. *Mol. Phys.* **1986**, *57* (1), 187-191.

[53] Hoover, W. G. Canonical dynamics: Equilibrium phase-space distributions. *Phys. Rev. A* **1985**, *31* (3), 1695-1697.

[54] Parrinello, M.; Rahman, A. Crystal Structure and Pair Potentials: A Molecular-Dynamics Study. *Phys. Rev. Lett.* **1980**, *45* (14), 1196-1199.

[55] Berendsen, H. J. C.; Postma, J. P. M.; van Gunsteren, W. F.; DiNola, A.; Haak, J. R. Molecular dynamics with coupling to an external bath. *J. Chem. Phys.* **1984**, *81* (8), 3684-3690.

[56] Bussi, G.; Donadio, D.; Parrinello, M. Canonical sampling through velocity rescaling. *J. Chem. Phys.* **2007**, *126* (1),

[57] Rickert, P. G.; Antonio, M. R.; Firestone, M. A.; Kubatko, K.-A.; Szreder, T.; Wishart, J. F.; Dietz, M. L. Tetraalkylphosphonium polyoxometalates: electroactive, “task-specific” ionic liquids. *Dalton Trans.* **2007**, (5), 529-531.

[58] Martinetto, Y. Development of new Ionic Liquids-based Polyoxometalates as oxidation catalysts applied to the recovery of biomass. Université Paris-Saclay, 2020.

[59] Rickert, P. G.; Antonio, M. R.; Firestone, M. A.; Kubatko, K.-A.; Szreder, T.; Wishart, J. F.; Dietz, M. L. Tetraalkylphosphonium Polyoxometalate Ionic Liquids: Novel, Organic−Inorganic Hybrid Materials. *J. Phys. Chem. B* **2007**, *111* (18), 4685-4692.

[60] Parker, Q.; Bell, R. G.; H. de Leeuw, N. Structural and dynamical properties of ionic liquids: a molecular dynamics study employing DL_POLY 4. *Mol. Simul.* **2019**, *47* (2-3), 152-160.

[61] Sun, Z.; Liu, X.; Zheng, L.; Cheng, T.; Kalhor, P.; Huai, Z.; He, Q.; Li, Y. Accurate modelling of pyrrolidinium ionic liquids with charge and vdW scaling. *J. Mol. Liq.* **2023**, *386*, 122541.

[62] Morrow, T. I.; Maginn, E. J. Molecular Dynamics Study of the Ionic Liquid 1-n-Butyl-3-methylimidazolium Hexafluorophosphate. *J. Phys. Chem. B* **2003**, *107* (34), 9160-9160.

[63] Zeron, I. M.; Abascal, J. L. F.; Vega, C. A force field of Li^+, Na^+, K^+, Mg^{2+}, Ca^{2+}, Cl^-, and SO_4^{2-} in aqueous solution based on the TIP4P/2005 water model and scaled charges for the ions. *J. Chem. Phys.* **2019**, *151* (13),

[64] Leontyev, I. V.; Stuchebrukhov, A. A. Electronic continuum model for molecular dynamics simulations. *J. Chem. Phys.* **2009**, *130* (8),

[65] Wang, Y.-L.; Sarman, S.; Li, B.; Laaksonen, A. Multiscale modeling of the trihexyltetradecylphosphonium chloride ionic liquid. *Phys. Chem. Chem. Phys.* **2015**, *17* (34), 22125-22135.

[66] Roy, D.; Maroncelli, M. An Improved Four-Site Ionic Liquid Model. *J. Phys. Chem. B* **2010**, *114* (39), 12629-12631.

[67] Canongia Lopes, J. N.; Deschamps, J.; Pádua, A. A. H. Modeling Ionic Liquids Using a Systematic All-Atom Force Field. *J. Phys. Chem. B* **2004**, *108* (30), 11250-11250.

[68] Shannon, R. Revised effective ionic radii and systematic studies of interatomic distances in halides and chalcogenides. *Acta Crystallographica Section A* **1976**, *32* (5), 751-767.

[69] Fogarty, Richard M.; Rowe, R.; Matthews, R. P.; Clough, M. T.; Ashworth, C. R.; Brandt, A.; Corbett, P. J.; Palgrave, R. G.; Smith, E. F.; Bourne, R. A.; et al. Atomic charges of sulfur in ionic liquids: experiments and calculations. *Faraday Discuss.* **2018**, *206* (0), 183-201.

[70] Fogarty, R. M.; Matthews, R. P.; Ashworth, C. R.; Brandt-Talbot, A.; Palgrave, R. G.; Bourne, R. A.; Vander Hoogerstraete, T.; Hunt, P. A.; Lovelock, K. R. J. Experimental validation of calculated atomic charges in ionic liquids. *J. Chem. Phys.* **2018**, *148* (19),

[71] Schmidt, J.; Krekeler, C.; Dommert, F.; Zhao, Y.; Berger, R.; Site, L. D.; Holm, C. Ionic Charge Reduction and Atomic Partial Charges from First-Principles Calculations of 1,3-Dimethylimidazolium Chloride. *J. Phys. Chem. B* **2010**, *114* (18), 6150-6155.

[72] Wang, X.; Liu, M.; Li, Y.; Zhang, Z.-y.; Zhuang, Y.; Sun, Z. Multi-temperature charge scaling of ionic solvents: Disparate responses of thermodynamic properties. *J. Mol. Liq.* **2024**, *409*, 125445.

[73] Liu, X.; Turner, C. H. Computational study of the electrostatic potential and charges of multivalent ionic liquid molecules. *J. Mol. Liq.* **2021**, *340*, 117190.

[74] Zhang, Y.; Zhang, Y.; McCready, M. J.; Maginn, E. J. Evaluation and Refinement of the General AMBER Force Field for Nineteen Pure Organic Electrolyte Solvents. *J. Chem. Eng. Data* **2018**, *63* (9), 3488-3502.

[75] Zhang, Y.; Otani, A.; Maginn, E. J. Reliable Viscosity Calculation from Equilibrium Molecular Dynamics Simulations: A Time Decomposition Method. *J. Chem. Theory Comput.* **2015**, *11* (8), 3537-3546.

[76] Hess, B. Determining the shear viscosity of model liquids from molecular dynamics simulations. *J. Chem. Phys.* **2002**, *116* (1), 209-217.

[77] Rey-Castro, C.; Vega, L. F. Transport Properties of the Ionic Liquid 1-Ethyl-3-Methylimidazolium Chloride from Equilibrium Molecular Dynamics Simulation. The Effect of Temperature. *J. Phys. Chem. B* **2006**, *110* (29), 14426-14435.

[78] López, X.; Fernández, J. A.; Poblet, J. M. Redox properties of polyoxometalates: new insights on the anion charge effect. *Dalton Trans.* **2006**, (9), 1162-1167.

[79] Solé-Daura, A.; Poblet, J. M.; Carbó, J. J. Structure–Activity Relationships for the Affinity of Chaotropic Polyoxometalate Anions towards Proteins. *Chemistry – A European Journal* **2020**, *26* (26), 5799-5809.

[80] Solé-Daura, A.; Notario-Estévez, A.; Carbó, J. J.; Poblet, J. M.; de Graaf, C.; Monakhov, K. Y.; López, X. How Does the Redox State of Polyoxovanadates Influence the Collective Behavior in Solution? A Case Study with $[I@V_{18}O_{42}]^{q-}$ (q = 3, 5, 7, 11, and 13). *Inorg. Chem.* **2019**, *58* (6), 3881-3894.